JOURNAL OF Materials CHEMISTRY

Low temperature synthesis, structure and magnetic properties of $La_{0.85}(Na_{1-x}K_x)_{0.15}MnO_3$ perovskites: the role of A cation size disparity in the electronic properties of mixed-valence manganates

Z. El-Fadli,[a]† E. Coret,[a] F. Sapiña,*[a] E. Martinez,[a] A. Beltrán,[a] D. Beltrán[a] and F. Lloret[b]

[a]*Institut de Ciència dels Materials de la Universitat de València, Apartado de Correos 2085, E-46071 València, Spain. E-mail: fernando.sapina@uv.es*
[b]*Departament de Química Inorgánica, Universitat de València, C/Doctor Moliner 50, E-46100 Burjassot, Spain*

Received 10th March 1999, Accepted 1st June 1999

Single-phase perovskites in the solid solution series $La_{0.85}(Na_{1-x}K_x)_{0.15}MnO_3$ ($0 \leqslant x \leqslant 1$) have been obtained using a soft treatment, which makes possible strict stoichiometric control. X-Ray powder diffraction patterns of these compounds have been completely indexed with a rhombohedral perovskite cell. The crystal structures have been refined in space group *R*-3*c*, in the hexagonal setting, from room-temperature data. Substitution of Na^+ by larger K^+ ions produces a cell expansion and a decrease in the structural distortion from the ideal cubic structure. The critical temperature for the paramagnetic–ferromagnetic transition, T_c, is found to be practically constant, *ca.* 333 K, along the entire series. This behaviour is unexpected, taking into account previous correlations established for the alkaline-earth $La_{0.7}(Ca_{1-x}Sr_x)_{0.3}MnO_3$ series (T_c increases with the mean size of cations at the A positions, $\langle r_A \rangle$) which expands over a similar $\langle r_A \rangle$ range. We can therefore discuss these results in terms of two counterweighting contributions: increasing T_c values could be expected as a consequence of the increase with x of the $\langle r_A \rangle$ value, but the concomitant disorder introduced at the A positions [as represented by the variance of the A cations radial distribution, $\sigma^2(\langle r_A \rangle)$] would cause a decrease in T_c. An approach to the understanding of the contribution that the electronic energy makes to this last effect is advanced.

Introduction

During the last decade there has been a renewed interest in doped rare-earth manganates owing to the discovery of colossal magnetoresistance (CMR) in $Ln_{1-x}A_xMnO_{3\pm\delta}$ (Ln = La, Pr, Nd, Sm; A = Ca, Sr, Ba) materials.[1] While the magnetic and electric properties of this type of material have been known for a long time,[2] the search for a satisfactory model accounting for CMR has given rise to systematic explorations intended to understand the basic aspects of the underlying interaction mechanism between manganese ions.

A remarkable result from these studies was the observation of the importance of the mean manganese ion oxidation state, having its optimum value (*i.e.* that leading to a maximum value of the critical temperature for the paramagnetic–ferromagnetic transition, T_c) close to 3.3.[3] Moreover, a relationship between T_c and the mean size of cations at the A sites, $\langle r_A \rangle$, was observed for $Ln_{0.7}A_{0.3}MnO_3$ samples with such a concentration (*ca.* 30%) of Mn^{4+}.[4] This notwithstanding, the matter is not simple, and more recent studies on related $Ln_{0.7}A_{0.3}MnO_3$ samples have shown that, in series with a fixed $\langle r_A \rangle$ value, T_c depends on disorder at the A sites [as represented by the variance of the A cationic radial distribution, $\sigma^2(\langle r_A \rangle)$].[5] At this point, it should be noted that recent results indicate that the critical temperature and phase diagram of $Ln_{0.5}A_{0.5}MnO_3$, and the critical temperature of $(Ln_{1-x}M_x)_2CuO_4$ superconductors also depend on $\langle r_A \rangle$ and $\sigma^2(\langle r_A \rangle)$.[5c,6,7] We cannot forget, however, that other factors such as the electronegativity of the alkaline-earth ions,[8] and the magnetic moments of ions at the A sites,[9] have also been described as influencing the electronic properties of this type of material. In addition, we have shown that by introducing vacancies in the B perovskite sites (while maintaining a constant concentration of Mn^{4+}, *ca.* 33%), as occurs for alkali-metal-doped manganates, $Ln_{1-x}A_xMnO_{3+\delta}$ (A = Na, K; $0 \leqslant x \leqslant 0.15$), the resulting electronic properties can be controlled by altering the concentration of vacancies at B positions.[10]

From all the above, it seems evident that CMR is a multivariable intricate phenomenon and much more work will still be needed to achieve a unified approach to understanding all the various factors involved. We present here new data for the $La_{0.85}(Na_{1-x}K_x)_{0.15}MnO_3$ series, *i.e.* a series (with no vacancies at B sites) along which both $\langle r_A \rangle$ and $\sigma^2(\langle r_A \rangle)$ values continuously vary with x. Indeed, we report on the synthesis, structure and magnetic properties of compounds in this series, which have been prepared using a low temperature method that makes possible reliable stoichiometric control.[10] As set out below, the critical temperature of these samples remains practically constant (*ca.* 333 K), regardless of the x (or $\langle r_A \rangle$) value. This is an initially unexpected result and it is qualitatively explained in terms of the counterweighting effects of the simultaneous increase with x of both $\langle r_A \rangle$ and $\sigma^2(\langle r_A \rangle)$ values. Finally, we advance a theoretical approach towards the rationalization of the effects of disorder on the electronic properties of mixed-valence manganates.

Experimental

Aqueous solutions of metal acetates with nominal molar compositions La : Na : K : Mn = 0.85 : 0.15(1 − *x*) : 0.15*x* : 1.00, with $x = 0.00$, 0.20, 0.40, 0.60, 0.80 and 1.00, were prepared as follows. $NaHCO_3$ and/or $KHCO_3$ were dissolved in 100 mL of glacial acetic acid. The addition of La_2O_3 led to a suspension, which was gently heated while stirring for 15 min. After addition of 20 mL of H_2O, a transparent solution resulted. After cooling, $Mn(CH_3COO)_2{\cdot}4H_2O$ was added and dissolved upon stirring. The masses of the different reagents were adjusted to give 5 g of perovskite. Droplets of the resulting

†On leave from the Département de Chimie, Faculté des Sciences, Université Abdelmalek Essaadi, Tétouan, Maroc.

pink pale acetic acid solutions were flash frozen by projection on liquid nitrogen and then freeze-dried at a pressure of 10^{-4} atm. In this way, dried solid precursors were obtained as loose pink powders.

Preliminary investigations have shown that the minimum temperature at which the perovskite phase is obtainable is 700 °C (12 h) for all compositions investigated in this work, and these conditions were thus adopted for thermal treatment of the perovskite precursors. After cooling in the furnace, the samples were ground, pelletized and heated under oxygen flow at 900 °C for 48 h.[11]

Metal contents were determined by atomic absorption using a Perkin-Elmer 300 AA spectrophotometer. The mean oxidation state of manganese ions, and thus the oxygen content, was determined by redox back-titration of Fe(II) with potassium dichromate in HCl using a Crison CompacT Titrator.

Powder diffraction patterns were obtained with a Siemens D501 diffractometer, using secondary graphite-monochromated Cu-Kα radiation. To reduce preferred orientation, the samples were dusted through a sieve on the holder surface. X-Ray data analyses were performed using the FULLPROF program.[12] Graphical representations concerning X-ray powder diffraction patterns were produced using the DRXWin program.[13]

Magnetization measurements were performed on a pendulum-type susceptometer in the temperature range 77–300 K at 1.23 T. Magnetization measurements at 77 and 300 K were performed working with magnetic fields up to 1.0 T. Transition temperatures were determined by thermogravimetric experiments, carried out using a Perkin-Elmer 7 system, with the samples under a small magnetic field.[14]

Results

Chemical and structural characterization

Table 1 summarizes the results of the chemical analyses. As can be seen, the mean manganese oxidation state is practically constant along the entire $La_{0.85}(Na_{1-x}K_x)_{0.15}MnO_3$ series, being 3.34 ± 0.02. As a consequence, δ is practically equal to zero (lower, in all cases, than 0.04), and the concentration of vacancies at A and B positions is therefore negligible. On the other hand, previous work on the synthesis, structural and electronic characterization of samples in the series $La_{1-x}A_xMnO_{3+\delta}$ (A = Na, K) has shown that, under the experimental conditions reported in this work, the nominal cationic stoichiometry is maintained during the preparative procedure.[10]

X-Ray powder diffraction patterns shown in Fig. 1 for $La_{0.85}(Na_{1-x}K_x)_{0.15}MnO_3$ were completely indexed in the rhombohedral perovskite-type structure. The structures of the perovskite phases have been refined in space group *R*-3*c*, in the hexagonal setting, from room-temperature X-ray powder diffraction data. The initial structural model used was that of $La_{0.95}Mn_{0.95}O_3$.[15] The fits were performed using a pseudo-Voigt peak-shape function. In the final runs, the usual profile parameters (scale factors, background coefficients, zero-points, half-width, pseudo-Voigt and asymmetry parameters for the peak-shape) and atomic positions were refined. Isotropic thermal parameters were set at 0.3 and 0.7 Å^2 for metal and oxygen atoms, respectively, and an overall thermal parameter was also refined. In the structural models, La, Na and K are considered to be randomly distributed in the A sites, and their occupancies were fixed to give the oxygen stoichiometry and metal contents obtained by chemical analysis. Refined structural parameters and residuals, R_p, R_{wp}, R_B and R_F, together with χ^2 values, are listed in Table 2. R_p and R_{wp} are the conventional (background corrected) peak only Rietveld profile and weighted profile residuals. R_B and R_F are the integrated intensity and structure factor residuals, respectively. χ^2 is the square of the goodness-of-fit indicator. In Table 3 a selected list of bond distances and angles, as well as cell parameters for the rhombohedral setting, are summarized.

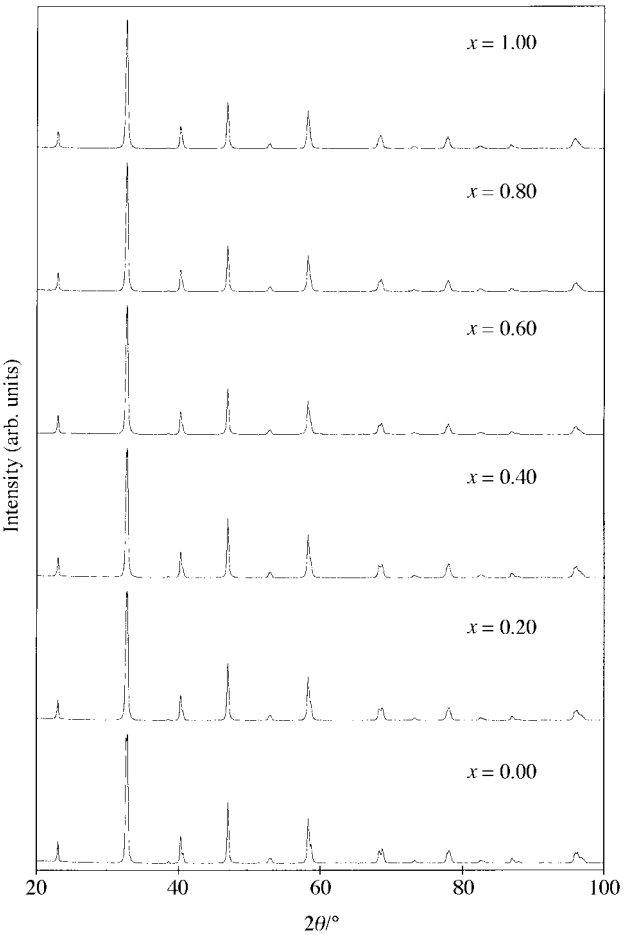

Fig. 1 X-Ray powder diffraction patterns of $La_{0.85}(Na_{1-x}K_x)_{0.15}MnO_3$.

Magnetic properties

We have measured hysteresis loops $M(77\ K, H)$ with fields up to 7000 Oe, after cooling in zero magnetic field. The knee of magnetization is reached at 2000 Oe, above that the magnetization changes linearly with the field. A linear extrapolation at

Table 1 Chemical analyses for samples of nominal composition $La_{0.85}(Na_{1-x}K_x)_{0.15}MnO_3$

	x					
	0.00	0.20	0.40	0.60	0.80	1.00
La/Mn	0.86(1)	0.84(1)	0.85(1)	0.85(1)	0.84(1)	0.85(1)
Na/Mn	0.15(1)	0.11(1)	0.09(1)	0.07(1)	0.02(1)	—
K/Mn	—	0.04(1)	0.06(1)	0.10(1)	0.13(1)	0.16(1)
$\%Mn^{4+}$	31(1)	32(1)	35(1)	35(1)	36(1)	36(1)
δ	0.02(3)	−0.01(3)	0.03(3)	0.04(3)	0.02(3)	0.04(3)

Table 2 Structural data for the X-ray powder diffraction studies of $La_{0.85}(Na_{1-x}K_x)_{0.15}MnO_3$

	x					
	0.00	0.20	0.40	0.60	0.80	1.00
a/Å	5.4936(3)	5.4949(3)	5.4979(3)	5.4987(4)	5.5001(3)	5.5036(3)
c/Å	13.3356(7)	13.3467(8)	13.3584(8)	13.3680(10)	13.3789(10)	13.3945(10)
x_O	−0.5438(10)	−0.5424(10)	−0.5406(11)	−0.5394(12)	−0.5377(12)	−0.5375(11)
R_p (%)	8.20	7.92	8.62	9.13	8.74	8.40
R_{wp} (%)	9.37	9.06	10.3	9.81	9.67	9.96
R_B (%)	2.82	2.41	3.12	1.68	1.76	2.08
R_F (%)	2.16	1.64	2.28	1.91	1.64	1.39
χ^2	1.82	1.77	1.73	1.40	1.41	1.58

Space group R-3c, hexagonal setting. La, Na, K (6a): (0, 0, $\frac{1}{4}$); Mn (6b): (0, 0, 0); O (18e): (x, 0, $\frac{1}{4}$).

Table 3 Selected bond distances (Å), angles (°) and cell parameters for the rhombohedral cells of $La_{0.85}(Na_{1-x}K_x)_{0.15}MnO_3$

	x					
	0.00	0.20	0.40	0.60	0.80	1.00
Mn–O (×6)	1.951(3)	1.951(3)	1.951(3)	1.951(3)	1.951(3)	1.953(3)
Mn–O–Mn	165.8(2)	166.3(3)	166.9(3)	167.2(2)	167.8(3)	167.9(3)
A–O (×6)	2.741(2)	2.742(2)	2.743(2)	2.744(2)	2.745(3)	2.748(3)
(×3)	2.987(4)	2.981(4)	2.972(4)	2.966(4)	2.957(5)	2.958(5)
(×3)	2.506(4)	2.514(4)	2.526(4)	2.533(4)	2.543(5)	2.545(5)
a_r/Å	5.46074(5)	5.46419(6)	5.46837(6)	5.47124(7)	5.47467(7)	5.48008(7)
α_r/°	60.3985(2)	60.3722(2)	60.3576(2)	60.3323(3)	60.3075(3)	60.2842(3)
V_r/Å^3	116.181(9)	116.333(10)	116.562(10)	116.680(13)	116.834(12)	117.120(12)

Table 4 Spontaneous magnetization and characteristic temperatures obtained from magnetization and TGA under a small magnetic field

	x					
	0.00	0.20	0.40	0.60	0.80	1.00
M_S/emu g^{-1} at 77 K	3.19	3.10	3.04	3.16	3.11	3.15
T_c/K	333	333	332	333	335	331

$H=0$ has enabled us to derive the spontaneous magnetization, M_S (77 K). In all samples the observed spontaneous magnetization is very close to the theoretical spontaneous magnetization, M_S^{calc} (3.68 μ_B), calculated considering the actual mixed valence of Mn ions in these compounds. These results are summarized in Table 4. Fig. 2 shows the isothermal magnetization (and a detail of the low field hysteresis curve) of the sample $x=1.00$ at 77 K. The values of the coercive fields are practically constant for all the compounds, being 75 ± 5 Oe at 77 K, and 25 ± 5 Oe at 295 K.

The temperature dependence of the magnetization was measured at a field of 12 kOe during warming runs, at temperatures ranging between 77 and 300 K. The magnetization decreases as the temperature increases and the abrupt drop corresponding to the transition from ferromagnetic to paramagnetic states is not observed due to the fact that the transition temperature is above 300 K.

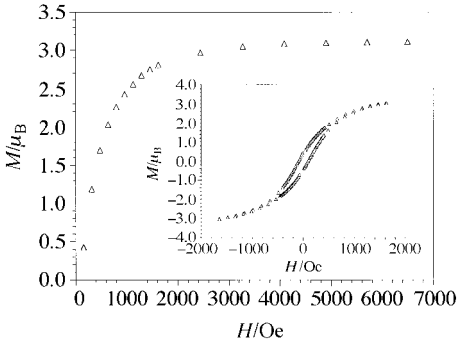

Fig. 2 Field dependence of the magnetization at 5 K, M (μ_B), for the $La_{0.85}Na_{0.15}MnO_3$ sample. The inset shows a hysteresis loop for this sample.

The ferromagnetic phase transition temperature for samples in the $La_{0.85}(Na_{1-x}K_x)_{0.15}MnO_3$ series was determined by means of thermogravimetric experiments performed under a small magnetic field.[14] The weight variation with temperature reflects the variation of the magnetization with temperature, and allows the determination of T_c. Fig. 3 shows the evolution

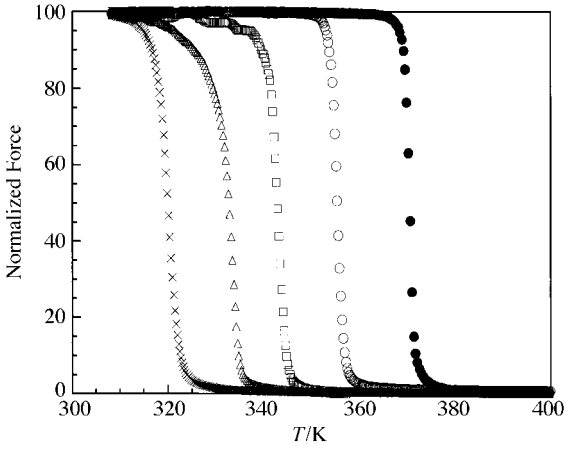

Fig. 3 Thermal variation of the normalized force for $La_{0.85}(Na_{0.2}K_{0.8})_{0.15}MnO_3$ (triangles) and $La_{0.7}(Ca_{1-x}Sr_x)_{0.3}MnO_3$ ($x=0.4$, 0.6, 0.8 and 1.0; crosses, squares, open circles and filled circles, respectively). Values of weight gain below T_c are typically in the 2–4% range. Such a dispersion can be attributed to differences in sample geometry. Then, the experimental values have been normalized to facilitate the comparison.

of the normalized force with temperature for samples in the series $La_{0.7}(Ca_{1-x}Sr_x)_{0.3}MnO_3$ (with $x=0.4$, 0.6, 0.8 and 1.0), as references, and $La_{0.85}(Na_{0.2}K_{0.8})_{0.15}MnO_3$, as a representative of the nearly coincident curves for the $La_{0.85}(Na_{1-x}K_x)_{0.15}MnO_3$ series. Such curves are indicative of the accuracy of the thermogravimetric method, which has allowed us to determine that the critical temperature is practically constant (333 ± 2 K) for all the samples in the $La_{0.85}(Na_{1-x}K_x)_{0.15}MnO_3$ series.

A representation of the reduced magnetization [$M(H, T)/M(H, 0\ K)$] *versus* the reduced temperature T/T_c is shown in Fig. 4. $M(H, 0\ K)$ is the magnetization extrapolated to 0 K obtained from the fit of the magnetization curve in the 77–150 K range with the expression predicted from the spin-wave theory.[16] All the samples present practically the same behaviour, as might be expected.

Discussion

Unlike the ideal cubic structure, the rhombohedral structure presents an irregular 12-coordination around the A cations, and a B–O–B angle that deviates substantially from 180°. Lattice effects on the electronic properties of mixed-valence manganates are particularly well documented,[4] and we will deal with them first. Fig. 5 shows the relationship between the rhombohedral cell volume, V_r, and the composition in the $La_{0.85}(Na_{1-x}K_x)_{0.15}MnO_3$ series. As can be seen, V_r monotonically increases with x. Also, the rhombohedral distortion with respect to the ideal cubic structure (as represented by α_r, the rhombohedral angle, and the Mn–O–Mn angle) decreases as x increases, as shown in Fig. 6 and Table 3. In practice, this behaviour is as expected, taking into account that K^+ ions are larger than Na^+ ions.

The relation between T_c and $\langle r_A\rangle$ for the $La_{0.85}(Na_{1-x}K_x)_{0.15}MnO_3$ and $La_{0.7}(Ca_{1-x}Sr_x)_{0.3}MnO_3$ series is plotted in Fig. 7(a). Values of $\langle r_A\rangle$ have been calculated as the weighted average of crystal radii for coordination number 9.[17] As can be seen, the dependence of T_c on $\langle r_A\rangle$ clearly differs from one series to another. Although, in good agreement with literature values,[4] the critical temperature for samples in the alkaline-earth series increases continuously with $\langle r_A\rangle$ (from 260 K for $La_{0.7}Ca_{0.3}MnO_3$ to 372 K for $La_{0.7}Sr_{0.3}$-

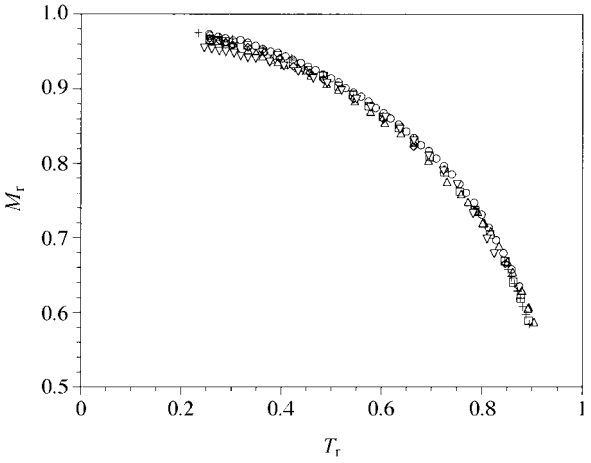

Fig. 4 Thermal variation of the reduced magnetization, $M(H, T)/M(H, 0\ K)$, *versus* the reduced temperature, T/T_c, for $La_{0.85}(Na_{1-x}K_x)_{0.15}MnO_3$ ($H=1.23$ T; down-triangles, circles, squares, crosses, rhombi and up-triangles correspond to data for $x=$ 0.00, 0.20, 0.40, 0.60, 0.80 and 1.00, respectively).

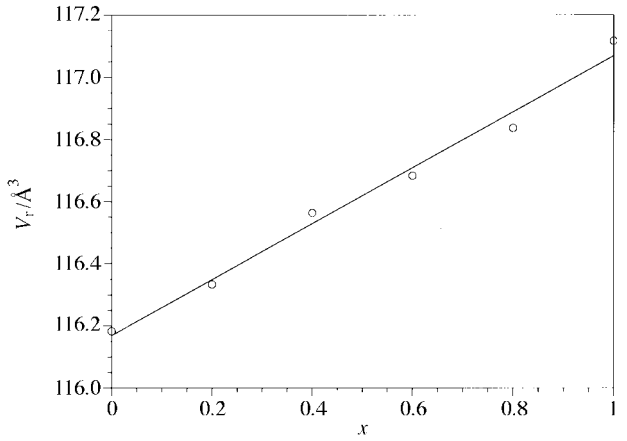

Fig. 5 Rhombohedral cell volume *versus* composition for $La_{0.85}(Na_{1-x}K_x)_{0.15}MnO_3$.

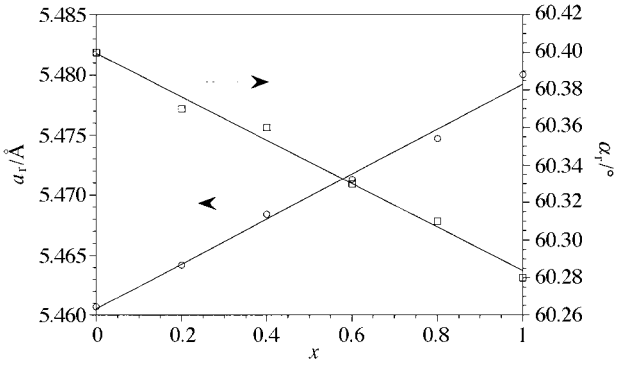

Fig. 6 Rhombohedral cell parameters a_r (circles) and α_r (squares) *versus* composition for $La_{0.85}(Na_{1-x}K_x)_{0.15}MnO_3$.

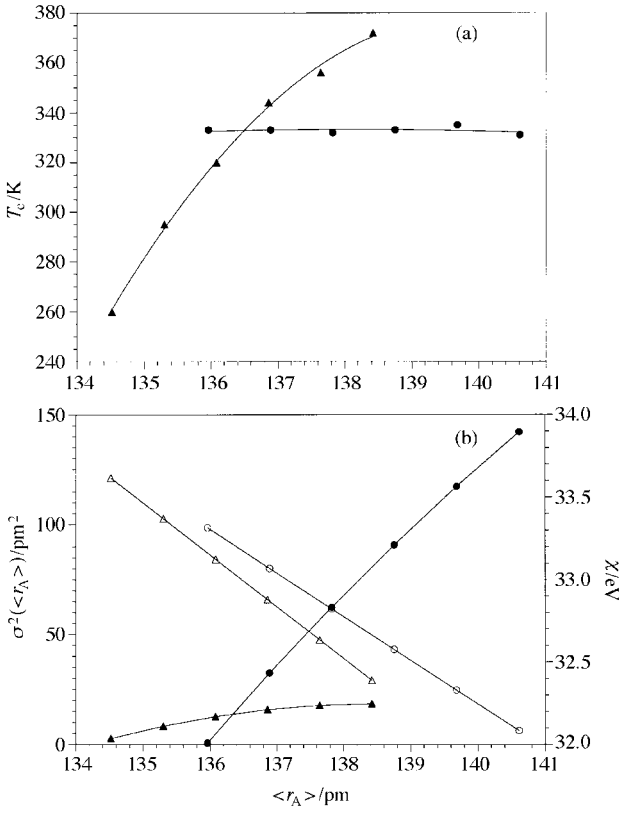

Fig. 7 (a) Critical temperatures, T_c, *versus* mean size of cations at the A sites, $\langle r_A\rangle$, for $La_{0.85}(Na_{1-x}K_x)_{0.15}MnO_3$ (closed circles) and $La_{0.7}(Ca_{1-x}Sr_x)_{0.3}MnO_3$ (closed triangles). (b) Variance of the A cations radial distribution, $\sigma^2(\langle r_A\rangle)$, (closed symbols) and mean absolute electronegativity of cations at A sites in the Pearson scale, χ_A, (open symbols) *versus* mean size of cations at the A sites, $\langle r_A\rangle$ for $La_{0.85}(Na_{1-x}K_x)_{0.15}MnO_3$ (circles) and $La_{0.7}(Ca_{1-x}Sr_x)_{0.3}MnO_3$ (triangles).

MnO_3), in the case of the alkali-metal series T_c remains practically constant regardless of the $\langle r_A \rangle$ value. This last result may seem rather surprising at first. In fact, as mentioned above, the results of previous work led us to correlate the values of the critical temperature of this type of compound (which have a constant concentration of Mn^{4+}, close to the optimum value, and an insignificant concentration of vacancies) with a range of factors. A major factor whose influence is widely recognized is $\langle r_A \rangle$. The $\langle r_A \rangle$ values determine, in practice, the structural distortion of the perovskite structure, or equivalently, the Mn–O–Mn angle and hence the spin-independent transfer integral (b) between Mn^{3+} and Mn^{4+} ions. The increase in T_c with $\langle r_A \rangle$ as Sr^{2+} replaces Ca^{2+} in $La_{0.7}A_{0.3}MnO_3$ has been linked to the subsequent decrease in the structural distortion of the perovskite structure. As our current observations for $La_{0.85}(Na_{1-x}K_x)_{0.15}MnO_3$, a series which extends over ranges of $\langle r_A \rangle$ values similar to those of the $La_{0.7}A_{0.3}MnO_3$ derivatives (see below), deviate from the above, it will be necessary to search for other effects which account for this. In this context, there is also abundant information indicating that the disorder at the A positions [given by $\sigma^2(\langle r_A \rangle)$] is another relevant factor influencing T_c: the induced local deformations of the MnO_6 octahedra act as 'performed Jahn–Teller distortions' which localize the e_g electrons, thereby lowering T_c.[5] On the other hand, the electronegativity of the cations at the A positions was also thought to affect T_c by modifying the effective ferromagnetic coupling.[8] This effect should be due to the fact that the s and p orbitals of the A cations would compete against the Mn t_{2g} orbitals for the electronic density of the O $2p_\pi$ orbitals. Finally, it has been also shown that the T_c values can be affected by the presence of magnetic ions in the A positions.[9] In any case, as the A cations are diamagnetic for all the compounds we are dealing with, this last effect must be obviated.

To consider the possible contributions of the above mentioned effects on T_c variation, we have represented in Fig. 7(b) both the mean absolute electronegativity[18] of the cations at the A sites (χ_A) and the variance of the A cations radial distribution [$\sigma^2(\langle r_A \rangle)$] as functions of $\langle r_A \rangle$. $\sigma^2(\langle r_A \rangle)$ quantifies the random disorder of La^{3+} and A^+ or A^{2+} cations distributed over the A perovskite sites. The data in Fig. 7(b) refer to both the $La_{0.85}(Na_{1-x}K_x)_{0.15}MnO_3$ and $La_{0.7}(Ca_{1-x}Sr_x)_{0.3}MnO_3$ series. As can be seen, the values of χ_A and $\langle r_A \rangle$ vary between similar limits. However, it will be noted that, for a given $\langle r_A \rangle$ value, the χ_A value corresponding to the alkali-metal series is higher than that of the alkaline-earth series. Thus, if the conclusions of Fontcuberta *et al.*[8] are generally applicable, the T_c value (for a given $\langle r_A \rangle$) should be higher for $La_{0.85}(Na_{1-x}K_x)_{0.15}MnO_3$ than for $La_{0.7}(Ca_{1-x}Sr_x)_{0.3}MnO_3$. This is not the case [Fig. 7(a)] and it seems evident that the electronegativity does not determine the observed behaviours for these series in the terms previously discussed.[8] On the other hand, the $\sigma^2(\langle r_A \rangle)$ values present different variation modes for both series. The total variation of $\sigma^2(\langle r_A \rangle)$ *versus* $\langle r_A \rangle$ is very small along the alkaline-earth series (2.7–18.6), but it is significantly larger in the case of the alkali-metal series (0.7–142.2). In this last case, such a variation of $\sigma^2(\langle r_A \rangle)$ should result in a significant decrease in T_c along the series, according to the literature data.

At this point, it seems reasonable to conclude that there are two counterweighting effects contributing to the observed experimental behaviour [Fig. 7(a)] of T_c in the $La_{0.85}(Na_{1-x}K_x)_{0.15}MnO_3$ series (*i.e.* to the constant value of T_c regardless of $\langle r_A \rangle$): the increase in T_c that might be expected as $\langle r_A \rangle$ increases[4] should be compensated for by the concomitant increase in $\sigma^2(\langle r_A \rangle)$.[5] Actually, a similar explanation might be suggested by the fact that $La_{0.7}Ba_{0.3}MnO_3$ has a T_c value (330 K)[14] lower than that corresponding to $La_{0.7}Sr_{0.3}MnO_3$ (372 K), in spite of the lower distortion of the barium perovskite (*i.e.* a variation with $\langle r_A \rangle$ which is just the opposite of that discussed above for $La_{0.7}A_{0.3}MnO_3$ and $La_{0.7}A_{0.3}MnO_3$; substitution of Sr^{2+} by the larger Ba^{2+} ions results in this case in a significant increase in the difference between the A cation radii, $\sigma^2(\langle r_A \rangle)$, which would work against the effect of increasing $\langle r_A \rangle$).

As the above qualitative conclusion is completely empirical, it seems appropriate to jointly re-examine the information now available to progress in the understanding of what was referred to as 'the close analogy between the effects of cation size ($\langle r_A \rangle$) and disorder [$\sigma^2(\langle r_A \rangle)$]'[5c] on the electronic properties of mixed-valence manganates. In short, the first picture that emerges from consideration of the tendencies observed to date is that, besides the A cation size (tolerance factor) effects,[4] the electronic properties of these materials are very sensitive to disorder. This may affect the A sites,[5,19] or it can be introduced by the presence of vacancies in the B sublattice.[10]

While the explanation of the tolerance factor effects in terms of the spin-independent transfer integral variations is generally assumed,[4] to understand how the structural disorder influences the electronic properties of these manganates, and particularly the T_c variations which we have discussed, the significance of T_c should be taken into account. For a first order transition such as the paramagnetic insulator (PMI) to ferromagnetic metallic (FMM) example which we are dealing with,[20] T_c can be expressed as the quotient of the enthalpy and entropy variations associated with the transition, $T_c = \Delta H/\Delta S$. The transition entropy can be approximated by the magnetic entropy change, $\Delta S \approx \Delta S_m = k\ln(2\langle S \rangle + 1)$ and, consequently, it should be constant for a given concentration of Mn^{4+}. Thus, what must be evaluated are the possible contributions to the transition enthalpy. As the PMI–FMM transition also implies measurable structural changes,[21] the transition enthalpy can be thought of as resulting from three different contributions, namely electronic, magnetic and lattice strain contributions. Thus, we can write $\Delta H = \Delta H_e + \Delta H_m + \Delta H_l$; $\Delta S \approx \Delta S_m = \text{constant}$; $T_c = T_e + T_m + T_l$, where T_e, T_m and T_l are the electronic, magnetic and lattice strain contributions to the critical temperature.

There are two queries that immediately arise when considering these contributions, namely (a) their relative weights in the absolute enthalpy variation and (b) their respective dependencies with disorder. While the first question is inherently difficult to answer, there is now sufficient information to rationally approach the explanation of how the structural disorder affects each contribution. In fact, the problem becomes simplified since experimental observations indicate that the influence of the structural disorder on the magnetic contribution to the critical temperature (T_m) seems to be negligible.[22] In fact significant variations in the superexchange interactions cannot be expected as a consequence of the relatively small variations in the Mn–O bond parameters (*i.e.* Mn–O–Mn angle and Mn–O distance) attributable to structural disorder only. On the other hand, the lattice strain contribution has been thoroughly analyzed by Attfield in ref. 5(*c*). In this important work, Attfield develops a theoretical model showing how, like the experimental T_c values, the T_l values (which depend on the mean Mn–O bond force) decrease linearly with $\sigma^2(\langle r_A \rangle)$ for a given value of $\langle r_A \rangle$, which initially also suggests an important lattice strain contribution to T_c. Although Attfield states that it is difficult to account for the effects of structural disorder in an electronic picture, it seems clear that the electronic contribution to the critical temperature, T_e, which must also be relevant, should show a dependence on [$\sigma^2(\langle r_A \rangle)$] analogous to that of T_c and T_l, *i.e.* a linear dependence.[23] The rest of our discussion is intended to develop a theoretical model on the basis of which such a dependence could be explained.

In accordance with the theoretical approach of Sheng *et al.*,[24] the electronic contribution to the transition enthalpy (and consequently T_e) is mainly caused by the spin dependence of

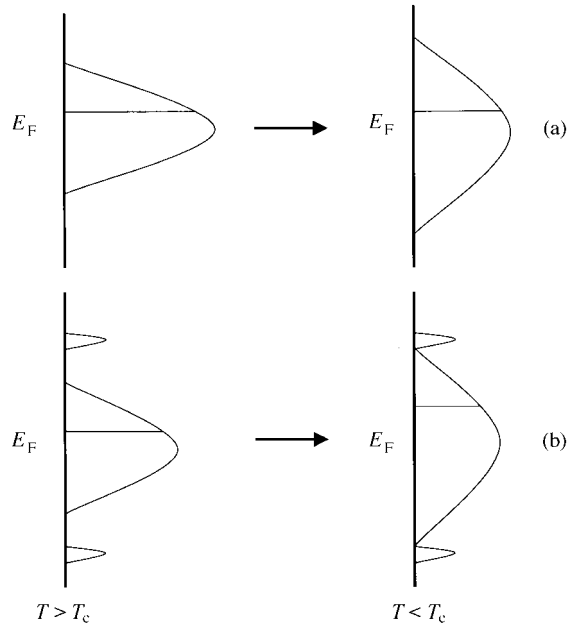

Fig. 8 Density of states (DOS) of the conduction band in mixed-valence manganates, for temperatures below and above T_c. (a) No structural disorder; (b) situation with structural disorder.

the transfer integral, t, which can be written as $t = b\cos(\theta_{ij}/2)$, where b is the spin-independent transfer integral and θ_{ij} is the angle between spins on neighboring Mn atoms.[25] Within this model, the electronic contribution to the transition enthalpy can be approached by eqn. (1),

$$\Delta H_e = E_{PM} - E_{FM} \approx \int \mathrm{DOS}_{PM}(E)\, f(E-\mu_{PM})\, E\, dE - \int \mathrm{DOS}_{FM}(E)\, f(E-\mu_{FM})\, E\, dE \quad (1)$$

where PM and FM represent the paramagnetic and ferromagnetic phases, respectively, E_i is the electronic energy, $\mathrm{DOS}_i(E)$ is the density of states in the conduction band and $f(E-\mu_i)$ is the Fermi–Dirac distribution function with chemical potentials μ_i, determined from the condition of fixed hole concentration.[24] The conduction band in mixed valence manganates is an antibonding σ^* band of e_g orbital parentage. In the absence of structural disorder, the spin order is at a maximum in the FM phase, and the width of the conduction band is $W_{FM} = 12b$. As the temperature increases, the spin disorder increases slowly until T_c, at which point it increases abruptly, reaching a maximum in the PM phase. Li *et al.* have calculated the width of the conduction band in the PM phase which turns out to be $W_{PM} = 8b$.[26] The electronic contribution to the critical temperature, T_e, should be directly related to b. The electronic structure in the vicinity of the Fermi level can be schematized for the PM and FM phases, as shown in Fig. 8(a). Zero in the energy scale is taken at the middle of the bands. Then, the band edges corresponding to the PM and FM phases are located at $\pm 4b$ and $\pm 6b$, respectively.

As a consequence of structural disorder, a fraction of the states in the conduction band become located beyond the original band edges, in energy intervals defined by $\pm[6b, 6b + W/2]$ for both PM and FM phases, where W is the disorder energy [Fig. 8(b)]. Within this framework, the disorder should be equally able to locate electrons below the bottom of the band and holes above the top of the band.[24]

Let us assume that the distribution of states beyond band edges is independent of the ordering of the magnetic moments, and that the form of the DOS curve inside the band edges is not substantially modified by the disorder. Then, if y is the fraction of states located beyond the band edges, we can write

$$\mathrm{DOS}_{i,D}(E) = (1-y)\,\mathrm{DOS}_{i,O}(E) \qquad i = \mathrm{PM},\ \mathrm{FM} \quad (2)$$

where $\mathrm{DOS}_{i,D}(E)$ and $\mathrm{DOS}_{i,O}(E)$ are the density of states in the i phase for the disordered (D) and ordered (O) cases, respectively, in the energy interval $-6b \leqslant E \leqslant 6b$. Under these assumptions, the condition

$$T_{e,D} = (1-y)\, T_{e,O} \quad (3)$$

is easily derived from eqn. (1).

The effect of structural disorder is, therefore, to reduce the electronic contribution, T_e, to the critical temperature, T_c. Other factors being equal, the fraction of states located beyond the band edges will increase with the disorder energy, and consequently, T_e will decrease. As $[\sigma^2(\langle r_A \rangle)]$ represents a measure of the structural disorder,[5c] it can be assumed that there is a direct proportionality between $[\sigma^2(\langle r_A \rangle)]$ and y, which results in eqn. (4)

$$T_{e,D} = T_{e,O}\,[1 - a\,\sigma^2(\langle r_A \rangle)] \quad (4)$$

and a linear decrease of the electronic contribution to the critical temperature with $[\sigma^2(\langle r_A \rangle)]$ is then expected.

Eqn. (4) can be further developed to explicitly show the dependence on $\langle r_A \rangle$ of the electronic contribution to T_c. In fact, such dependence is included in the $T_{e,O}$ parameter. Thus, as stated above, $T_{e,O}$ is proportional to b. In turn, b varies with $\cos\omega$, where $\omega = 1/2(\pi - \Theta)$, and Θ is the Mn–O–Mn angle. Using the hard sphere model proposed by Attfield,[5c] in which all A cations are considered as equal spheres having the average $\langle r_A \rangle$ radius, the oxygen atom displacements with respect to the ideal cubic structure (which would exist for a given value, r_A^0, of the A cation radius), are given by $Q = r_A^0 - \langle r_A \rangle$. As a consequence, $\sin[1/2(\pi - \Theta)] = [r_A^0 - \langle r_A \rangle]/d$, where d is the Mn–O distance. As the values of ω are small, $\sin\omega$ can be approached by ω, and $\cos\omega$ by $1 - \omega^2/2$. As a consequence, b is proportional to $1 - c(r_A^0 - \langle r_A \rangle)^2$, and substitution in eqn. (4) gives eqn. 5.

$$T_{e,D} = T_e[1 - a\,\sigma^2(\langle r_A \rangle)][1 - c(r_A^0 - \langle r_A \rangle)^2] \quad (5)$$

As will be noted, this expression for the electronic contribution to the critical temperature is, as could not occur in any other way, analogous to that proposed by Attfield[5c] in order to account for the lattice strain contribution. Then, both the linear dependence of the electronic contribution on $\sigma^2(\langle r_A \rangle)$ [for a given $\langle r_A \rangle$ value] and the effect of $\langle r_A \rangle$ on T_e [for a given $\sigma^2(\langle r_A \rangle)$ value] which eqn. (5) predicts, are consistent with the experimental observations concerning the T_c values. T_c, T_1 and T_e all show analogous dependencies on the two key parameters $\langle r_A \rangle$ and $\sigma^2(\langle r_A \rangle)$. As both of these parameters will simultaneously vary in the same sense, their effects on T_1 and T_e, and consequently on T_c, will work one against the other. The fact that in the $La_{0.85}(Na_{1-x}K_x)_{0.15}MnO_3$ series this results in a 'perfect' balance leading to a constant T_c value, can initially be considered as a happy coincidence which has allowed us to explore in more detail the role of the A cation size disparity in the electronic properties of mixed-valence manganates.

Acknowledgements

This research was supported by the Spanish Comisión Interministerial de Ciencia y Tecnología (CICYT, MAT96-1037). Z. El-Fadli is grateful to the Instituto de Cooperación con el Mundo Arabe and the Universitat de València for grants. The SCSIE of the Universitat de València is acknowledged for X-ray diffraction and analytical facilities.

References

1 (*a*) R. M. Kusters, J. Singleton, D. A. Keen, R. McGreevy and W. Hayes, *Physica B*, 1989, **155**, 362; (*b*) R. von Helmot, J. Wecker, B. Holzapfel, L. Schultz and K. Samwer, *Phys. Rev. Lett.*, 1993, **71**, 2331; (*c*) S. Jin, T. H. Tiefel, M. McCormack,

R. A. Fastnacht, R. L. Ramesh and H. Chen, *Science*, 1994, **64**, 413.
2 (*a*) Z. Zener, *Phys. Rev.,* 1951, **82**, 403; (*b*) P. W. Anderson, *Phys. Rev.*, 1955, **100**, 675; (*c*) P. G. De Gennes, *Phys. Rev.*, 1960, **116**, 141.
3 (*a*) P. Schiffer, A. P. Ramirez, W. Bao and S. W. Cheong, *Phys. Rev. Lett.*, 1995, **75**, 3336; (*b*) A. Urushibara, Y. Moritomo, T. Arima, A. Asamitsu, G. Kido and Y. Tokura, *Phys. Rev. B*, 1995, **51**, 14103.
4 (*a*) A. Maignan, V. Caignert, Ch. Simon, M. Hervieu and B. Raveau, *J. Mater. Chem.*, 1995, **5**, 1091; (*b*) H. Y. Hwang, S. W. Cheong, P. G. Radaelli, M. Marezio and B. Batlogg, *Phys. Rev. Lett.*, 1995, **75**, 914; (*c*) R. Mahesh, R. Mahendiran, A. K. Raychaudhuri and C. N. R. Rao, *J. Solid State Chem.*, 1995, **120**, 204; (*d*) J. Fontcuberta, B. Martinez, S. Piñol, J. L. García-Muñoz and X. Obradors, *Phys. Rev. Lett.*, 1996, **76**, 1122.
5 (*a*) L. M. Rodriguez-Martinez and J. P. Attfield, *Phys. Rev. B*, 1996, **54**, R15622; (*b*) L. M. Rodriguez-Martinez and J. P. Attfield, *Phys. Rev. B*, 1998, **58**, 2426; (*c*) J. P. Attfield, *Chem. Mater.*, 1998, **10**, 3239.
6 (*a*) F. Damay, C. Martin, A. Maignan and B. Raveau, *J. Appl. Phys.*, 1997, **82**, 6181; (*b*) B. Raveau, A. Maignan, C. Martin and M. Hervieu, *Chem. Mater.*, 1998, **10**, 2641.
7 J. P. Attfield, A. L. Kharlanov and J. A. McAllister, *Nature*, 1998, **394**, 157.
8 J. Fontcuberta, B. Martinez, S. Piñol, J. L. García-Muñoz and X. Obradors, *Phys. Rev. B*, 1997, **55**, R668.
9 J. Xu, W. H. Tang and J. K. Liang, *J. Phys.: Condens. Matter*, 1998, **10**, 1387.
10 (*a*) Y. Ng-Lee, F. Sapiña, E. Martinez-Tamayo, J. V. Folgado, R. Ibañez, D. Beltrán, F. Lloret and A. Segura, *J. Mater. Chem.*, 1997, **7**, 1905; (*b*) T. Boix, F. Sapiña, Z. El-Fadli, E. Martinez, A. Beltrán, J. Vergara, R. J. Ortega and K. V. Rao, *Chem. Mater.*, 1998, **19**, 1569; (*c*) J. Vergara, R. J. Ortega-Hertogs, V. Madurga, F. Sapiña, Z. El-Fadli, E. Martinez, A. Beltrán and K. V. Rao, *Phys. Rev. B*, in press.
11 Samples in the series $La_{0.7}(Ca_{1-x}Sr_x)_{0.3}MnO_3$ (with $x=0.0$, 0.2, 0.4, 0.6, 0.8 and 1.0) and $La_{0.7}Ba_{0.3}MnO_3$, which are used for comparison, were obtained by using the same preparative procedure.
12 J. Rodriguez-Carvajal, FULLPROF Program, personal communication.
13 V. Primo, DRXWin and CreaFit version 2.0, graphical and analytical tools for powder XRD patterns, *Powder Diffr.*, 1999, **14**, 70.
14 Transition temperatures for $La_{0.7}Ba_{0.3}MnO_3$ and samples in the series $La_{0.7}(Ca_{1-x}Sr_x)_{0.3}MnO_3$ were also obtained by thermogravimetric experiments, except for the $x=0.0$ and 0.2 samples (which have transition temperatures lower than 300 K). In these last cases, the transition temperatures were determined by ac susceptibility measurements performed using a Lake Shore Cryotonics Inc. Model 7000 ac susceptometer (temperature range 100–325 K, frequency and exciting field, 333 Hz and 1 Oe, respectively). All the experimental results concerning these compounds are in good agreement with those previously reported in the literature for analogous compositions (ref. 4).
15 J. A. M. Van Roosmalen, E. H. P. Cordfunke, R. B. Helmholdt and H. W. Zandbergen, *J. Solid State Chem.*, 1994, **110**, 100.
16 A. H. Morris, *The Physical Principles of Magnetism*, Robert E. Kreiger Publishing Company, New York, 1980.
17 R. D. Shannon, *Acta Crystallogr., Sect. A*, 1976, **32**, 751.
18 R. G. Pearson, *Inorg. Chem.*, 1988, **27**, 734.
19 F. Millange, V. Caignert, B. Domengès and B. Raveau, *Chem. Mater.*, 1998, **10**, 1974.
20 W. Archibald, J. S. Zhou and J. B. Goodenough, *Phys. Rev. B*, 1996, **53**, 14445.
21 (*a*) P. G. Radaelli, G. Iannone, M. Marezio, H. Y. Hwang, S. W. Cheong, J. D. Jorgensen and D. N. Argyriou, *Phys. Rev. B*, 1997, **56**, 8265; (*b*) V. Caignert, E. Suard, A. Maignan, Ch. Simon and B. Raveau, *C. R. Acad. Sci.*, *Ser. IIb*, 1995, **321**, 515.
22 J. M. De Teresa, M. R. Ibarra, J. García, J. Blasco, C. Ritter, P. A. Algarabel, C. Marquina and A. del Moral, *Phys. Rev. Lett.*, 1996, **76**, 3392.
23 In fact, structural disorder in mixed valence manganates can be produced by the presence of at least two different cations at the A sites or, alternatively, be due to the presence of cationic vacancies at the B sites. The present discussion, as well as Attfield's analysis, is centered on the former source of structural disorder, which is consistent with the absence of cationic vacancies ($\delta \approx 0$) in the series we are dealing with. The effect of disorder produced by cationic vacancies is discussed elsewhere (ref. 10).
24 (*a*) L. Sheng, D. Y. Xing, D. N. Sheng and C. S. Ting, *Phys. Rev. Lett.*, 1997, **79**, 1710; (*b*) L. Sheng, D. Y. Xing, D. N. Sheng and C. S. Ting, *Phys. Rev. B*, 1997, **56**, 7053.
25 In fact, by assuming this approach, the electronic energy variations associated with the decrease in the Mn–O bond length due to the FM–PM transition are being neglected, and the change in the electronic energy associated with the transition is approximated by considering that only the energy of the more external (conduction band) states is modified. Such a simplification finds experimental support in previous results such as those of Radaelli *et al.* in ref. 21(*a*).
26 Q. Li, J. Zhang, A. R. Bishop and C. M. Soukoulis, *Phys. Rev. B*, 1997, **56**, 4541.

Paper 9/01904I